PERGAMON

International Journal of Solids and Structures 38 (2001) 4557–4570

INTERNATIONAL JOURNAL OF SOLIDS and STRUCTURES

www.elsevier.com/locate/ijsolstr

Boundary element method analysis of temperature fields in coated cutting tools

Fang Du, Michael R. Lovell *, Tim W. Wu

Department of Mechanical Engineering, University of Kentucky, Lexington, KY 40506-0108, USA

Received 2 August 1999; in revised form 7 July 2000

Abstract

Two general boundary element techniques are developed for determining the temperature fields in materials containing thin coatings. The first method utilizes a two-dimensional multi-domain approach that is accurate over a wide range of coating thicknesses. The second technique, which is based on a more computationally efficient single-layer approximation, is geared towards applications where the coating thickness is very small. After initially being verified with two simplified test cases, both methods are used to determine the temperature fields of coated and uncoated metal cutting tool inserts. Through generation of results for different coating materials (TiN, TiC, and Al_2O_3) and by comparison with actual experimental data, the accuracy and applicability of the single-domain approximation and multiple-domain methods are discussed as related to machining processes.

Keywords: Machining; Cutting temperature; Single layer approximation; Multi-domain approach

1. Introduction

Applications for thin coating films have increased immensely over the past several decades. With improvements in coating deposition techniques and the development of more advanced coating materials, coatings have pervaded numerous industries that include the automotive, computer, aerospace, and precision manufacturing. In the metal cutting industry, for example, almost all cutting tools are coated with thin layers of titanium carbide (TiC), titanium carbonitride (TiCN), titanium nitride (TiN), and aluminum oxide (Al_2O_3) to improve machining performance. Both single- and multiple-layer combinations of these films are deposited onto cemented carbide or high-speed steel tools using chemical (CVD) and physical (PVD) vapor deposition techniques. With better temperature- and wear-resistant properties than their

* Corresponding author. Present address: Department of Mechanical Engineering, University of Pittsburgh, 635 Benedum Engineering Hall, 3700 O'Hara Street, Pittsburgh, PA 15261, USA. Fax: +1-412-624-9601.

E-mail address: mlovell@pitt.edu (M.R. Lovell).

0020-7683/01/$ - see front matter
PII: S0020-7683(00)00291-2

substrate counterparts, cutting tool coatings not only prolong the life of the cutting tool but also improve the final surface quality of the workpiece. Looking specifically at different coating materials, TiC and Al_2O_3 materials possess ultrahigh hardness properties for wear resistance and have good chemical stability to provide a strong heat barrier between the tool and the formed chip. TiN, on the other hand, provides a lower coefficient of friction to the face of the tool insert which substantially reduces cratering of the cutting tool (Sandvik, 1996).

In the manufacturing community, a large percentage of machining processes are performed under high-speed and dry cutting conditions. For these conditions, extremely high temperatures are generated along the cutting edge of the tool. Such temperatures can lead to a form of chemical tool wear that is characterized by the dissolution and diffusion of the tool material into the workpiece material. In dry cutting, this type of chemical wear becomes the predominant mode of tool failure (Hoffman, 1984) where the tool life is relatively short. Cutting tool coatings have been found to be particularly beneficial for reducing chemical tool wear in dry cutting. Previous research (Dearnley, 1985) has shown that the maximum rake face temperature for TiN-coated tools was lower than uncoated tool grades under identical cutting conditions. Further work on dry cutting has shown that the effectiveness of different coating materials depends on the cutting speeds. Thomas and Donald (1981) found that Al_2O_3 resists wear better at high speeds, while TiC resisted wear better at lower speeds. In more recent work, Grzesik (1997, 1999) determined that the coating system structure significantly influenced the average tool–workpiece interface temperature at different cutting speeds and feed rates. Despite the significant contributions of each of the above works, it is important to note that they all were experimental in nature and focussed on observing the cutting temperature and wear for a certain set of operating conditions. In fact, to the author's knowledge, there does not exist any work in the literature for predicting the temperature distribution within a coated cutting tool. The objective of this paper is to develop a general boundary element program for determining the temperature distribution in thin coating layers that can be applied to the analysis of cutting tools.

With the great advancement of computer hardware over the past decade, numerical modeling techniques have become a widely accepted tool in the scientific community for solving previously intractable problems. In the area of calculating cutting tool temperature distributions, several publications have recently utilized the boundary element method (BEM). In the pioneering work in this area, Chandra and Chan (1994) analyzed the steady-state heat conduction problem using a two-dimensional boundary element approach. Stephenson et al. (1997) later expanded Chandra's work to perform numerical simulations of transient heat conduction problems in the machining using a three-dimensional approach. Notwithstanding the importance of both these articles, neither of the above numerical techniques considered tool coatings, which is the predominant method of cutting in the manufacturing community.

In this work, two general methods are introduced for evaluating the temperature field in a material containing a thin-layered coating. The first method utilizes a two-dimensional multi-domain boundary element approach that is applicable for a wide range of coating thicknesses. The second method, which is based on an efficient single-domain boundary element approximation, is best suited for very thin coating layers. After both the methods are developed, they are initially verified using a simplified geometry for which a known analytical solution exists. Once validated for this initial test case, the methods are then further verified by comparing predicted temperature distributions in an uncoated cutting tool for which the experimental temperature distribution is available. Finally, the accuracy and applicability of the single- and multi-domain methods are discussed as related to an analysis of a coated cutting tool system. It is important to note that only single-layered films of TiN, TiC, and Al_2O_3 are analyzed in this work to demonstrate the applicability of the single- and multi-domain methods. Since multi-layer coatings are more commonly used by the machining community, and single layers of Al_2O_3 are not generally produced, the authors plan to extend the numerical methods presented herein to the future work which will include multi-layer coatings.

2. Boundary integral formulations

2.1. Governing differential equation and boundary conditions

A schematic diagram of a machining process is sketched in Fig. 1 where the tool is moved into the workpiece. In this problem, the material undergoes a severe plastic deformation along the shear plane. As the chip forms, it diverts and slides across the tool face. There are three main regions of heat generation in machining: (1) the primary deformation zone where the chip is formed, (2) the secondary deformation zone where the chip slides over the tool cutting face, and (3) the area where the machined surface contacts the clearance face (flank) of the tool. The heat transfer mechanisms involved are conduction and convection to the environment of the heat generated in the tool.

For metal cutting processes, various tool force measurements and cine-photographs confirm that the machining process is essentially steady for a continuous strip (Chandra and Chan, 1994). This allows the transient part of the heat transfer problem to be set to zero. The grain sizes of the work material and the tool material are also quite small compared to the sizes of the deformation zones. Hence, the workpiece, tool, and chip may be treated as a continua, each of which is homogeneous and isotropic. It is also reasonable to assume that thermal conductivity, specific heat and density remain constant over the range of a typical metal cutting process (Chandra and Chan, 1994). If the temperature field is approximated to be two dimensional, the cutting tool insert can be considered the main section of the field to be calculated. The temperature in this region is governed by Laplace's equation:

$$\nabla^2 T = 0. \tag{1}$$

It is important to note that in coated cutting tools, Eq. (1) only applies within each layer of material separately because of differences in thermal conductivity.

In this work, orthogonal machining will be considered and a two-dimensional analysis of heat transfer will be performed. The following conditions have been assumed: (1) the tool temperature before cutting is at room temperature (25°C), and (2) the cutting edge is very sharp so that the heat produced along the machined surface within the clearance face (flank) of tool can be neglected. As shown in Fig. 2, the tool insert has two of its boundaries in contact with the tool holder (at $x_1 = L$, and $x_2 = 0$). In the previous works by Wu et al. (1992), Stephenson and Ali (1992), and Radulescu and Kapoor (1994), these boundaries

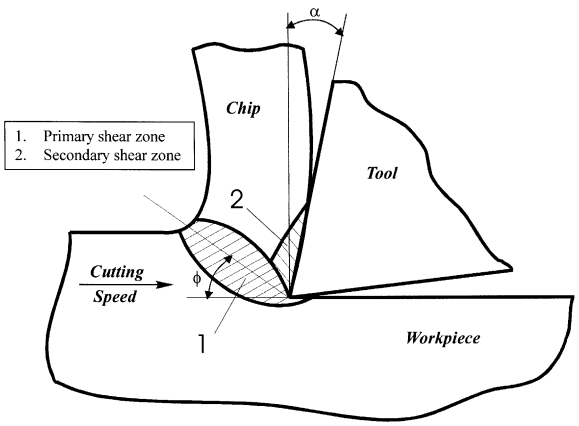

Fig. 1. Heat generation in a machining operation.

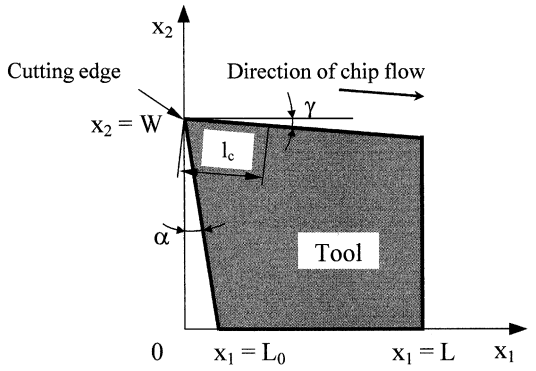

Fig. 2. The geometry of cutting tool in the calculation domain.

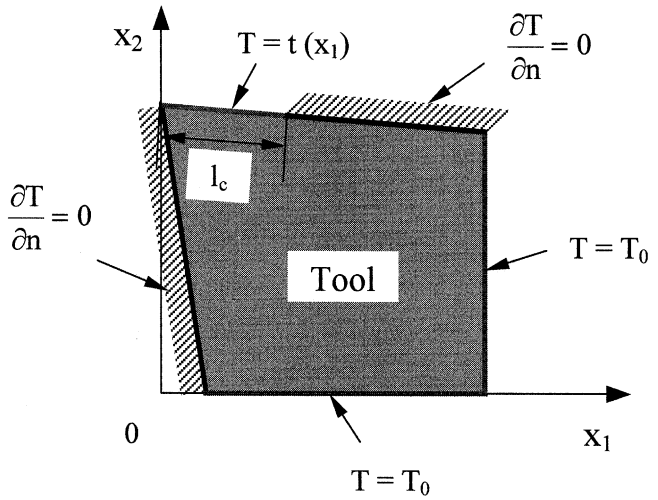

Fig. 3. Boundary conditions for the cutting tool.

were assumed to be at the ambient temperature (25°C). All the three works yielded temperatures at the tool–chip interface that were in reasonable agreement with the experimental results.

The other two boundaries of the tool insert (at $0 \leqslant x_1 \leqslant L$, $0 \leqslant x_2 \leqslant W$, and $x_2 = W$) are exposed to the environment (except where the tool is in contact with the chip). If dry cutting conditions are considered, the heat transfer to the air is typically negligible relative to the heat entering the tool (Wu et al., 1992; Jen and Lavine, 1994; Stephenson et al., 1997). Therefore, an insulation of $\partial T/\partial n = 0$ is imposed on these boundaries. All the boundary conditions used in this study are summarized in Fig. 3. The temperature distribution $T = t(x_1)$ at the tool–chip contact area will be determined from experimental measurements.

2.2. Multi-domain boundary element method

In the machining industry, most cutting tool inserts are designed with coatings that are deposited on the HSS or cemented carbide. These coatings consist of one layer or more layers. The thin film layers of coating protect the tool against adhesion, diffusion and intensive abrasive wear. They also provide a barrier for the intensive heat flowing from the contact area into the substrate material (Dearnley, 1985).

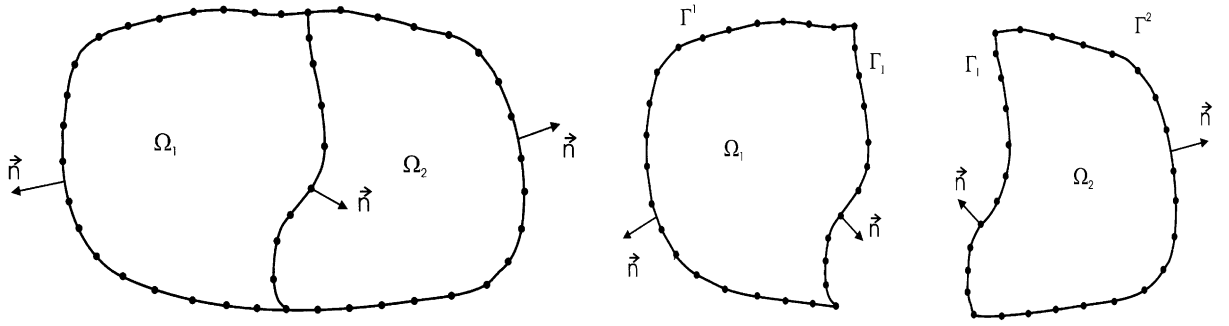

Fig. 4. Boundary discretization for two subdomains.

One way to model the tool insert with coatings is to use the multi-domain BEM (Brebbia, 1980). For simplicity, only one layer of coating is treated in this paper, although the formulation can be extended to multiple layers. A generic two-domain problem is illustrated in Fig. 4 where the entire domain is composed of two homogenous and isotropic subdomains. The coefficients of heat conductivity of two subdomains are denoted by K_1 and K_2, respectively. The exterior boundary of subdomain Ω_1 is Γ_1 and that of subdomain Ω_2 is Γ_2. The contact interface between the two subdomains is Γ_1. For each subdomain, the Laplace equation is satisfied and is converted into a boundary integral equation as follows:

For subdomain Ω_1,

$$C_1(P)\,T_1(P) = \int_{\Gamma_1+\Gamma_I} \left(\psi \frac{\partial T_1}{\partial n_1} - T_1 \frac{\partial \psi}{\partial n_1}\right) \mathrm{d}\Gamma. \tag{2}$$

For subdomain Ω_2,

$$C_2(P)\,T_2(P) = \int_{\Gamma_2+\Gamma_I} \left(\psi \frac{\partial T_2}{\partial n_2} - T_2 \frac{\partial \psi}{\partial n_2}\right) \mathrm{d}\Gamma, \tag{3}$$

where T_1 and T_2 are the temperatures in Ω_1 and Ω_2, respectively, n_1 and n_2, the outward normal vectors on the boundary, P, the collocation point, $C_1(P)$ and $C_2(P)$, the coefficients that depend on the location of P, and ψ, a fundamental solution. The expression for ψ in two dimensions is

$$\psi = -\frac{1}{2\pi} \ln r, \tag{4}$$

where r is the distance between the collocation point P and any point Q on the boundary. The coefficient $C_i(P)$ $(i = 1, 2)$ is equal to one for P in subdomain Ω_i, or zero for P outside subdomain Ω_i, or $1/2$ for P on the smooth part of the boundary $\Gamma_i + \Gamma_I$. In general, it can be evaluated by

$$C_i(P) = -\int_{\Gamma_i+\Gamma_I} \frac{\partial \psi}{\partial n_i} \mathrm{d}\Gamma. \tag{5}$$

Eqs. (2) and (3) are coupled by the two continuity conditions at the interface:

(a) Continuity of temperature

$$T_1 = T_2 \quad \text{on } \Gamma_I. \tag{6}$$

(b) Continuity of normal flux

$$K_1 \frac{\partial T_1}{\partial n_1} = -K_2 \frac{\partial T_2}{\partial n_2} \quad \text{on } \Gamma_I. \tag{7}$$

For a well-posed boundary value problem, there is only unknown (either T or $\partial T/\partial n$) at each nodal point on the exterior boundary. However, along the interface Γ_I, both T and $\partial T/\partial n$ are unknowns. To solve the problem numerically, the boundary of each subdomain is discretized into a number of elements and nodes as shown in Fig. 4. The two meshes need to match perfectly along the interface. Eq. (2) is then collocated at each nodal point on $\Gamma_1 + \Gamma_I$, and Eq. (3) is collocated at each nodal point on $\Gamma_2 + \Gamma_I$. For each collocation point, one algebraic equation is generated. Since Γ_I is shared by the two meshes, there are two algebraic equations (one generated by Eq. (2) and the other generated by Eq. (3) associated with each nodal location on the interface). Therefore, there will be the same number of algebraic equations as the unknowns. The system of equations can be solved simultaneously for the boundary and interface unknowns. Once the boundary unknowns are solved, Eqs. (2) and (3) can be integrated to obtain the temperature at any point inside each subdomain.

2.3. Single-domain approximation for thin-layer coating

The multi-domain BEM approach is inefficient when the coating is very thin. Under such a circumstance, the mesh on the exterior coating surface will be almost identical to the mesh on the interface. Unlike crack analysis problems where the integral equation becomes nearly singular (Liu, 1998), there will be no degeneracy of boundary integral equation for thin coatings. Either a very fine mesh with massive integration points or a special integration technique (Liu, 1998) needs to be adopted. In this work, a very efficient approximation method is proposed to avoid the integration difficulty for thin coatings.

Instead of modeling the very thin-layer coating using the BEM, an analytical model is used to approximate the heat conduction behavior in the coating layer. With reference to Fig. 5 the temperature at any point Q on the interface is denoted by T. The corresponding coating-surface temperature at point Q_p that is directly above Q is denoted by T_p. Then, the normal flux at point Q is approximated by the finite-difference expression

$$-K\frac{\partial T}{\partial n} = -K_c\frac{T_p - T}{h}, \tag{8}$$

where K is the coefficient of heat conduction for the substrate, K_c, the coefficient of heat conduction for the coating material, and h, the thickness of coating. The only approximation used in Eq. (8) is the finite-difference approximation to the normal derivative of temperature at the coating–substrate interface. Rearranging Eq. (8) gives

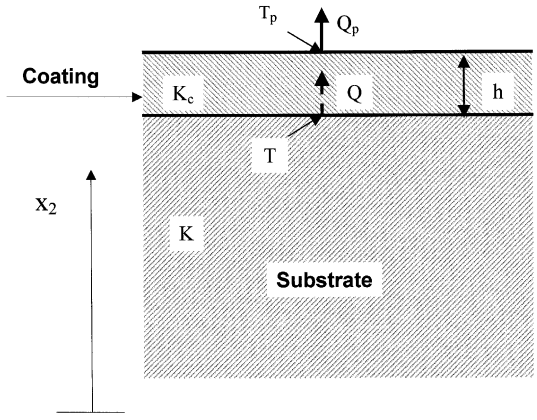

Fig. 5. Configuration of heat conduction for thin-layer coating.

$$T + \left(\frac{K}{K_c}h\right)\frac{\partial T}{\partial n} = T_p. \tag{9}$$

When T_p is specified, Eq. (9) can be used as the Robin boundary condition for the boundary-value problem defined for the substrate. Therefore, only the substrate needs to be modeled by the BEM. The coating effects are automatically included in the Robin boundary condition in Eq. (9).

On the other hand, if heat flux instead of temperature is prescribed on the coating surface, the boundary condition would be the same heat flux applied at the coating–substrate interface. In other words, the flux boundary condition on the substrate surface is

$$-K\frac{\partial T}{\partial n} = Q_c, \tag{10}$$

where Q_c is the prescribed heat flux on the coating surface.

A more complicated situation is when a convection boundary condition is prescribed on the coating surface. Assume that the original boundary condition on the coating is

$$\alpha T_c + \beta\frac{\partial T_c}{\partial n} = \gamma, \tag{11}$$

where α, β, and γ are specified coefficients and T_c is the temperature distribution in the coating. On solving T_c from Eq. (11), we get

$$T_c = \frac{\gamma}{\alpha} - \frac{\beta}{\alpha}\frac{\partial T_c}{\partial n} = \frac{\gamma}{\alpha} - \frac{\beta}{\alpha}\left(\frac{K}{K_c}\frac{\partial T}{\partial n}\right), \tag{12}$$

where the continuity of heat flux across the interface is used. On substituting Eq. (12) into Eq. (9), we get

$$T + \frac{K}{K_c}\left(h + \frac{\beta}{\alpha}\right)\frac{\partial T}{\partial n} = \frac{\gamma}{\alpha}. \tag{13}$$

Eq. (13) is the new boundary condition on the coating–substrate interface. Actually, the temperature boundary condition as stated in Eq. (9) is a special case of the general form of Eq. (13).

3. Verification of boundary element method results

Before proceeding to a more complex simulation of an actual machining process, two simplified coating test cases are introduced to establish the accuracy of the BEM techniques developed herein. In the first test case, which is depicted in Fig. 6, the mediums of domain Ω_1 and Ω_2 are assumed to respectively have heat conductivities of $K_1 = 1$ W/m K and $K_2 = 2$ W/m K. The domain Ω_1 will be considered to be the coating with a variable thickness, h. Both the vertical sides of domains Ω_1 and Ω_2 are assumed to be insulated so that there is no heat flux perpendicular to the lines along $x_1 = 0$ and $x_1 = 1$. From basic heat transfer theory, the analytical temperature solution for domain Ω_2 is given by

$$T(P) = \frac{K_1 x_2}{(K_2 - K_1)h + K_1 H}T_1 \quad (P \in \Omega_2), \tag{14}$$

where x_2 is the vertical location within Ω_2, H, the total height of the two domains, and T_1, the temperature on the top. On substituting $K_1 = 1$ W/m K, $K_2 = 2$ W/m K, $H = 1$ mm and $T_1 = 1$ K into Eq. (14), the exact solution becomes

$$T(P) = \frac{1}{1+h}x_2 \quad (P \in \Omega_2). \tag{15}$$

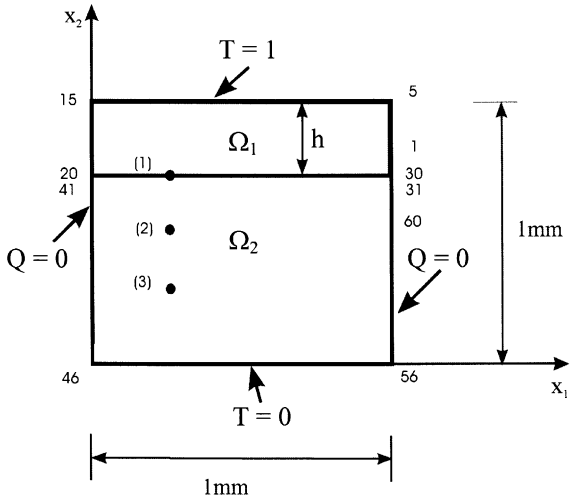

Fig. 6. Simple test case with one-dimensional heat transfer.

Using this analytical solution, the accuracy of both the single-domain approximate method and multi-domain BEM can be evaluated for thin coatings.

For the purpose of comparing the numerical and analytical results, the temperature distributions were evaluated in domain Ω_2 at 10 different coating thicknesses between 1 and 10 μm. It is important to note that thin-layer coatings of 1 μm are commonly used in the manufacturing community, particularly when coating high-speed steel tools. For these thin layers, however, PVD coating processes must be employed, and the variability of coating thickness along the tool can be significant. Specific comparisons were then made between temperatures at the following three points (Fig. 6):

(1) $x_1 = 0.3$, $x_2 =$ the interface of domain Ω_1 and Ω_2,
(2) $x_1 = 0.3$, $x_2 = 0.5$,
(3) $x_1 = 0.3$, $x_2 = 0.2$.

In each of the analyses, the boundary element mesh (depicted in Fig. 6) was identically modeled for the 10 coating thicknesses examined. As shown in Fig. 7(a)–(c), both the multi-domain and approximate BEMs yield highly accurate temperature results when compared with analytical values. In fact, as demonstrated by the figures, the approximate method yields more accurate results than the multi-domain method, especially for small coating thicknesses. Such a finding is significant because the approximate BEM, which is very computationally efficient, shows significant potential for analyzing thin solid coating problems, such as those found in the metal cutting industry.

Since the finite-difference approximation happens to be exact for the above simple one-dimensional test case, it is still not clear whether the approximation can be used under more complicated conditions. In the second test case, we construct a configuration that is closer to a real machining process. As shown in Fig. 8, a 7×7 mm^2 square with a thin coating of thickness, h, is used. The boundary conditions specified in Fig. 8 are complicated enough to ensure two-dimensional heat transfer. For different coating thickness values, the temperature at a domain point (1 mm, 6.41 mm) is recorded in Table 1 for the two different BEMs. Although there is no analytical solution to compare with for this test case, common sense can still be used in interpreting the data. Due to the lack of an analytical solution, the temperature difference between the two solutions is shown in the table. From the table, it is shown that the multi-domain solution begins to

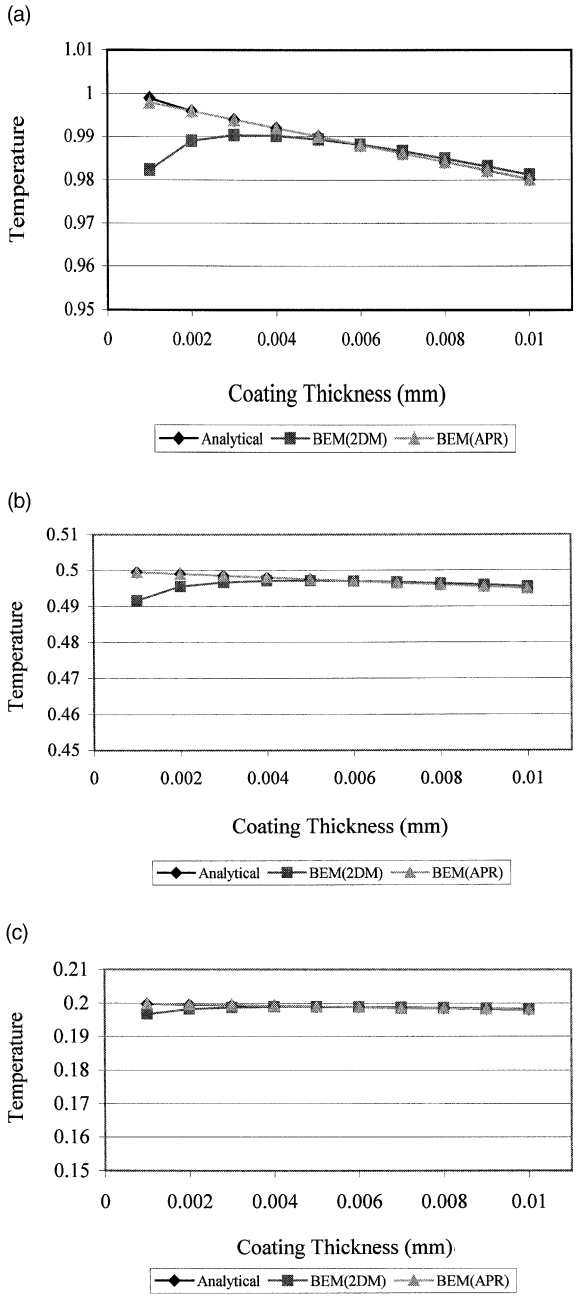

Fig. 7. Comparison of temperature distributions at selected points.

deteriorate (or refuses to keep increasing) as the coating thickness drops below 5 μm. On the other hand, the single-domain approximation solution does continue to show the correct upward trend. However, at the other end of the spectrum, the single-domain approximation starts to show its limitation as the coating thickness goes above 50 μm. Between 5 and 50 μm, the two solutions do agree with each other.

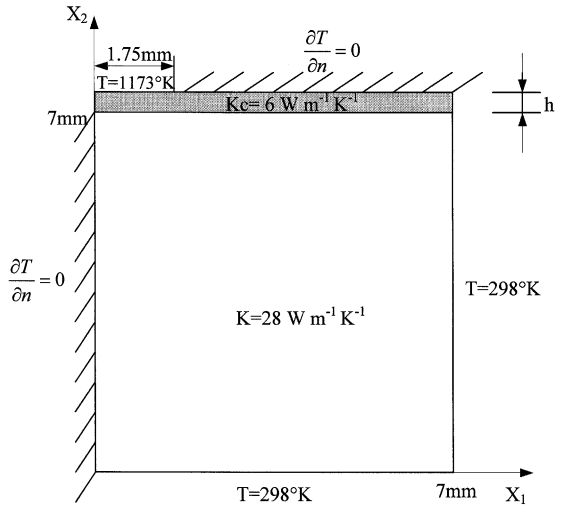

Fig. 8. Test case with two-dimensional heat transfer.

Table 1
Comparison of single- and multi-domain results for different coating thicknesses

Coating thickness (μm)	Multi-domain solution (K)	Single-domain approximation (K)	Temperature difference (K)
1	983.5	1016.5	33
2	998.8	1014.8	16
3	1003.5	1013.2	9.7
5	1011.1	1010.0	1.1
10	1004.2	1002.4	1.8
50	956.8	951.2	5.6
500	688.3	666.5	21.8
1000	572.1	547.0	25.1

4. Machining applications

4.1. Uncoated tool comparison

As a final step towards validating the BEM programs developed in this work, the temperature distribution in an uncoated tool will be determined by the approximate and multi-domain BEMs for a geometry for which experimental results are available. Fig. 9 shows the temperature distribution obtained by Kato et al. (1976) for an orthogonal machining process using the melting powder temperature measurement technique. In Kato's work, the tools used for the machining process were divided into two symmetric parts (parallel to the chip flow direction), and fine powders (10–20 μm size) of different salts were scattered on one side of divided surfaces. The tools were put back together and machining experiments were performed. Different types of powders were used to cover the temperature range of 473–1073 K so that a total temperature field could be established by superimposing results of different experiments. The resulting experimental field is plotted in Fig. 9 along with the numerically predicted temperatures. In order to obtain the BEM predicted values shown in Fig. 9, the temperature profile (maximum temperature of 1233 K) and contact length (1.75 mm) along the flank face of the cutting tool is needed to be input as boundary conditions to the boundary element programs. It is important to note that obtaining such a temperature

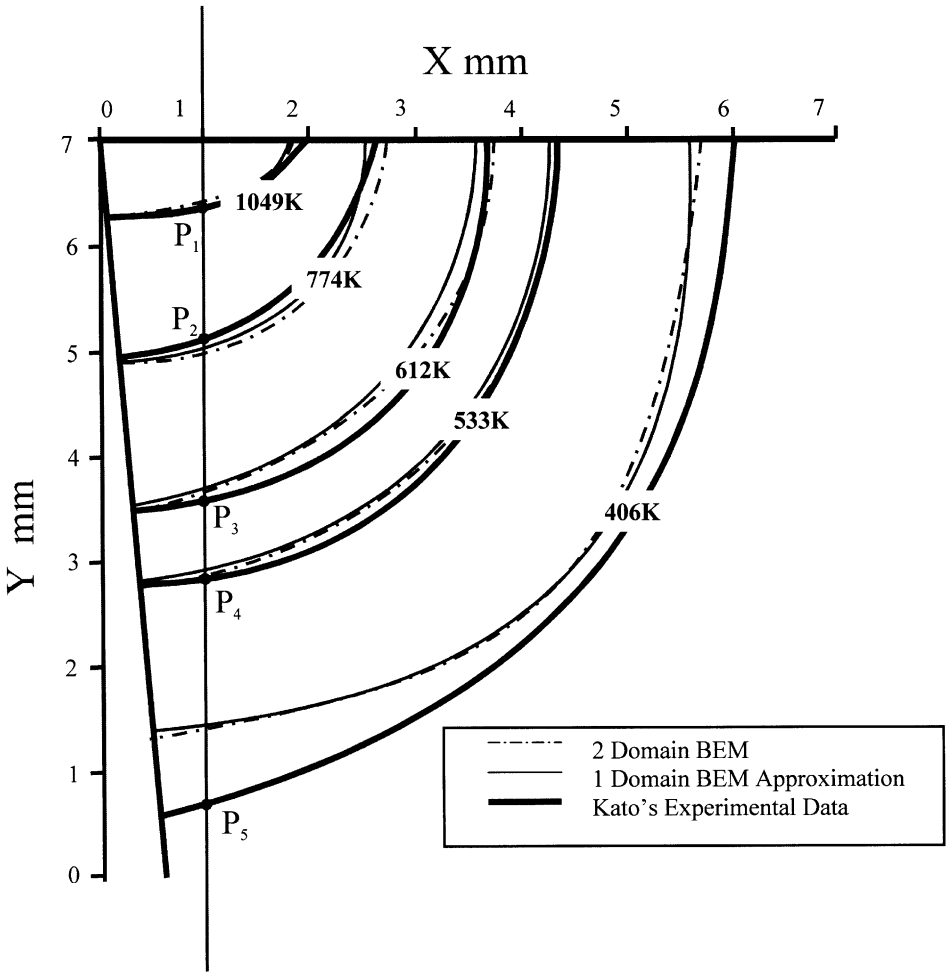

Fig. 9. Comparison of experimental and BEM results.

distribution along the tool–chip contact length is usually a fundamental task, as it very difficult to obtain such information using standard temperature measurement techniques. For the purpose of analyzing the numerical techniques developed in this work, the applied temperature distribution was directly obtained from Kato's results depicted in Fig. 9. The other boundary conditions used in the uncoated BEM analyses are depicted in Fig. 3 (coating thickness 5 μm). Since a Carbide (P20) cutting tool was used in Kato's experiments, a thermal conductivity value of $K = 46$ W/m K was assumed at a temperature of 1200 K. As shown, the bottom and right-hand side of the cutting tool were held at an ambient temperature of 298 K, and the portions of the rake and flank face not contacting the chip were insulated. With these boundary conditions, uncoated temperature distributions were obtained using identical material properties for the coatings and tool inserts. As shown in Fig. 9, the relatively small difference between the experimental and BEM predicted results demonstrate that the BEM can be considered an effective technique for determining the temperature distribution in cutting tools. The differences in temperature can be partially attributed to the fact that a constant value of the thermal conductivity was assumed for the tool and coating materials. In

Table 2
Comparison of single- and muti-domain results with experiments

Coating thickness (mm)	Temperature (K)			
	Multi-domain approximation		Single-domain approximation	
	Solution	Temperature difference	Solution	Temperature difference
0.001	1044.69	4.31	1044.43	4.57
0.003	1049.96	0.96	1044.11	4.89
0.005	1051.18	2.18	1042.96	6.04
0.007	1051.77	2.77	1042.26	6.74
0.01	1051.07	2.07	1041.24	7.76
0.015	1052.52	3.52	1041.54	7.46

Experimental datum for point (1.0, 6.429) is 1049 K.

reality, the thermal conductivity of coating and tool materials can significantly vary with temperature as many materials show a decrease in K of nearly 50% between 300 and 1000 K.

In order to further quantify the accuracy of both the approximate and multi-domain methods, seven different coating thicknesses were examined for the geometry depicted in Fig. 2. A comparison between the experimental data and the solutions from the approximate and multi-domain BEMs are given in Table 2 for the point $x_1 = 1.0$, $x_2 = 6.429$. As demonstrated by the table, both the approximate and multi-domain results show good correlation with the experimental values. In the single-domain results of Table 2, it is also found that the error increases with coating thickness. Such a finding is significant because it indicates the potential limitation of the approximate method for large coating thicknesses.

4.2. Coated tool results

For the purpose of demonstrating the applicability of the BEM techniques developed in this work, temperature distributions were determined for the geometry depicted in Fig. 4 for the coatings TiN, TiC, and Al_2O_3. Identical boundary conditions to that described in Section 4.1 were used with a coating thickness of 5 μm. The thermal properties of each coating are listed in Table 3. It is important to note at this point that applying the same contact length and temperature distribution boundary conditions for each coating is a simplification of a more complex set of variables. In practice, both the maximum temperature and the contact length will likely change with coating material and cutting conditions. In fact, as determined by Grzesik (1997, 1999), the coating material can significantly influence the chip–rake contact length. Since the focus of the current work is on the development of BEM techniques for analyzing the temperature distribution in coated tools, the influence of coating material on the contact length is not considered. Once established, however, the proposed numerical techniques could analyze variable contact lengths by simply modifying the boundary conditions. The determined temperature profiles from the two different BEM solutions are shown for each coating material in Tables 4 and 5 at five different locations within the cutting tool. The location of each point given in the tables are graphically shown in Fig. 9.

Table 3
Thermal properties of coating materials (Jawahir and van Luttervelt, 1993)

Coating	Coating technique	Thermal conductivity at ambient (W/m K)	Thermal conductivity at 1200 K (W/m K)
TiC	CVD	32	43
TiN	CVD	20	27
Al_2O_3	CVD	36	6

Table 4
Cutting tool temperature distribution for single-domain BEM at 5 μm coating thickness

Point	Location in tool, (X, Y) mm	Temperature (K)			
		Al_2O_3	TiN	TiC	Uncoated
P_1	(1.00, 6.41)	1027.986	1037.772	1038.860	1038.978
P_2	(1.00, 5.23)	795.997	803.023	803.812	803.899
P_3	(1.00, 3.64)	322.975	327.370	327.854	327.902
P_4	(1.00, 2.91)	595.013	598.415	598.764	598.800
P_5	(1.00, 0.63)	347.708	348.457	348.556	348.564

Table 5
Cutting tool temperature distribution for two-domain BEM at 5 μm coating thickness

Point	Location in Tool (X, Y) mm	Temperature (K)			
		Al_2O_3	TiN	TiC	Uncoated
P_1	(1.00, 6.41)	1029.564	1044.294	1045.988	1046.183
P_2	(1.00, 5.23)	800.419	810.952	812.232	812.383
P_3	(1.00, 3.64)	598.727	605.295	606.113	606.212
P_4	(1.00, 2.91)	527.568	523.638	533.272	533.349
P_5	(1.00, 0.63)	343.652	344.690	344.821	344.837

As demonstrated in the tables, the temperature distribution within the cutting tool is found to directly depend on the coating material. The TiC coating, for example, if found to have little or no influence on reducing the temperature distribution within the cutting tool. In fact, for all five points examined, the TiC coating case has nearly the same temperature as the uncoated case. The Al_2O_3 case, on the other hand, shows a moderate decrease in temperature compared to the uncoated case throughout the cutting tool. The final coating, TiN, is found to have a temperature distribution that falls somewhere in between the TiC and Al_2O_3 cases. Such a tendency can be explained by examining the thermal conductivity values of the coatings used in the present investigation. As given in Table 3, the thermal conductivity of the Al_2O_3 coating (6 W/m K) is significantly lower than the conductivity of the TiC (43 W/m K) and TiN (27 W/m K) coatings at elevated temperatures. Hence, with a low thermal conductivity value, the Al_2O_3 coating will act as a thermal barrier to the heat generated in machining and lower the cutting tool temperature distribution.

5. Summary and conclusions

In this work, the multi-domain and the single-domain boundary element techniques were developed for determining the temperature distribution in materials containing thin coating films. After being initially verified for a simplified test case, the two techniques are applied to the analysis of temperatures in cutting tool coatings. From the determined boundary element results, the following conclusions can be drawn:

(1) The single-domain approximation and multi-domain BEMs were found to accurately predict the temperature distribution in materials containing thin coatings. It was determined that both the methods could be effectively applied to the analysis of cutting tools in the machining industry.

(2) Despite requiring less computational resources, the single-domain approximation method was found to be very accurate under very thin coating conditions.

(3) Errors in the single-domain approximation results were found to increase at larger coating thicknesses. Such an increase indicates that the approximation technique is limited to fairly thin coating applications. The multi-domain method, on the other hand, was found to be more reliable as the coating

thickness increases. However, when the coating becomes extremely thin, more efforts and special integration techniques are needed to produce accurate results.

(4) The single- and multiple-domain BEMs predicted that the Al_2O_3 coating was much more effective than TiC in reducing the temperatures in the cutting tool during machining. This finding was in good agreement with the previous wear experiments quoted in the literature (Thomas and Donald, 1981) and has been described by Jawahir and van Luttervelt (1993) as the *thermal barrier effect*.

Acknowledgements

The authors would like to acknowledge the Design Manufacturing and Industrial Innovation Division of the National Science Foundation (grant no. DMI-9703196) for providing financial support and equipment for this work.

References

Brebbia, C.A., 1980. The Boundary Element Method for Engineers. Pentech Press, London, UK.

Chandra, A., Chan, C.L., 1994. Thermal aspects of machining: a BEM approach. Int. J. Solids Struct. 31 (12/13), 1657–1693.

Dearnley, P.A., 1985. Rake and flank wear mechanisms of coated cemented carbides. Surf. Engng. 1 (1), 43–58.

Grzesik, W., 1997. The role of coatings in controlling the cutting process when turning with coated indexable inserts. J. Mater. Process. Technol. 79, 133–143.

Grzesik, W., 1999. Experimental investigation of the cutting temperature when turning with coated indexable inserts. Int. J. Mach. Tools Manufact. 39, 355–369.

Hoffman, E.G., 1984. Fundamentals of Tool Design., second ed. Society of Manufacturing Engineers.

Jawahir, I.S., van Luttervelt, C.A., 1993. Recent developments in chip control research and applications. Ann. CIRP 42, 659–693.

Jen, T.C., Lavine, A.S., 1994. Prediction of tool temperatures in interrupted metal cutting, Proc. 7th Int. Symp. Transport Phenom. Manufact. Processes, pp. 221–216.

Kato, S., Yamagucho, K., Watanabe, Y., Hiraiwa, Y., 1976. Measurement of temperature distribution within tool using powders of constant melting point. J. Engng. Ind. 75-WA/Prod-5, pp. 1–7.

Liu, Y.J., 1998. Analysis of shell-like structures by the boundary element method based on 3-D elasticity: formulation and verification. Int. J. Numer. Meth. Engng. 41, 541–558.

Radulescu, R., Kapoor, S.G., 1994. An analytical model for prediction of tool temperature fields during continuous and interrupted cutting. ASME J. Engng. Ind. 116, 135–143.

Sandvik, C., 1996. Modern Metal Cutting.

Stephenson, D.A., Ali, A., 1992. Tool temperature in interrupted metal cutting. ASME J. Engng. Ind. 114, 127–136.

Stephenson, D.A., Jen, T.-C., Lavine, A.S., 1997. Cutting tool temperatures in contour turning: transient analysis and experimental verification. ASME J. Manufact. Sci. Engng. 119, 494–501.

Thomas, H., Donald, G., 1981. How effective are the carbide coatings. Modern Machine Shop, April, pp. 98–106.

Wu, J.S., Dillon, O.W., Lu, W.Y., 1992. Thermo-viscoplastic modeling of machining process using a mixed finite element method, ASME. Computational Method in Materials Processing, MD-Vol. 39/PED-Vol. 61, pp. 113–127.